CHEMBIOCHEM

DOI: 10.1002/cbic.200800353

Two-Photon Fluorescent Probes for Biomembrane Imaging: Effect of Chain Length

Hwan Myung Kim,[a, d] Bo Ra Kim,[a] Hyo-Jung Choo,[b] Young-Gyu Ko,[b] Seung-Joon Jeon,[a] Chul Hoon Kim,[c] Taiha Joo,*[c] and Bong Rae Cho*[a]

Two-photon fluorescent probes for the cellular membrane, derived from 6-acyl-2-aminonaphthalene as the fluorophore and hexanoyl (CH), lauryl (CL), and stearyl (CS) groups as the receptor, have been synthesized. Their photophysical properties and utility as membrane probes were also studied. Whereas CH cannot be used as a membrane probe due to its high water solubility, CL and CS are useful two-photon probes for membrane lateral heterogeneity, as they can easily stain cells, emit fluorescence with high sensitivity to the environment polarity, and are capable of imaging the membrane lateral heterogeneity in live cells. Moreover, CS is more likely to be located in the plasma membrane due to its negligible water solubility. Our results show that the liquid ordered-like domain covers 31–35% of the cellular surface.

Introduction

Currently there is interest in the development of efficient two-photon probes for application in two-photon microscopy (TPM). TPM, which employs two near infrared photons for excitation, has attracted much attention in biological imaging because it offers a number of advantages over one-photon microscopy (OPM), such as increased penetration depth (>500 μm), lower tissue auto-fluorescence and self absorption, and reduced photodamage and photobleaching.[1–3] The extra penetration that TPM affords is particularly important in avoiding artifacts of surface preparation in tissue imaging; cells damaged through preparation can extend >70 μm into the interior of brain slices.[4] However, most of the one-photon fluorescent probes presently used for TPM have small TP action cross-sections ($\Phi\delta$) that limit their use.[5,6] Therefore, there is a pressing need to develop efficient TP probes for specific applications.

K. Simons et al. proposed that ordered rigid domains of lipids (termed lipid rafts) exist on cell membranes. Lipid rafts are rich in cholesterol (CHL) and glycosphingolipids, and carry various membrane proteins and receptors.[7,8] Consequently, they serve as a platform to support the various biological functions of living cells.[9–14] However, the existence of such domains in biological membranes has never been proven.[15] Hence, it is important to develop new biophysical tools to study the lateral heterogeneity of the biological membrane. Recently, we reported a new membrane two-photon probe for membrane lateral heterogeneity, 6-dodecanoyl-2-[*N*-methyl-*N*-(carboxymethyl)amino]naphthalene (C-laurdan, CL). This probe showed several advantages over laurdan, including greater sensitivity to solvent polarity, brighter two-photon fluorescence images, and a more precise reflection of the cellular environment.[16] The stronger two-photon excited fluorescence (TPEF), the symmetrical generalized polarization (GP) distribution curve, which could be deconvoluted into two curves with similar shape and area, and the dramatic decrease in the high GP curve without changing the low one by treatment with methyl-β-cyclodextrin (MβCD) were found to have added usefulness. One of the drawbacks of this probe is that it not only stains membranes but also stains the cytosol. To develop a membrane probe that preferentially locates itself in the plasma membrane, we have designed a probe with longer hydrocarbon chain, 6-stearoyl-2-[*N*-methyl-*N*-(carboxymethyl)amino]-naphthalene (C-steardan, CS). Because the lipid raft is believed to be thicker than other parts of the plasma membrane,[17] this probe might have a preference for this domain due to favorable hydrophobic interactions. For comparison, the shorter chain analogue, 6-hexanoyl-2-[*N*-methyl-*N*-(carboxymethyl)amino]naphthalene (C-hexadan, CH) has also been studied.

In this paper, we present the synthesis of a series of CL derivatives with different chain lengths and the effects of the structural variations on the photophysical properties, GP distribution curves, and GP images in the vesicles and cell.

[a] *Dr. H. M. Kim, B. R. Kim, Prof. Dr. S.-J. Jeon, Prof. Dr. B. R. Cho*
Department of Chemistry and
Center for Electro- and Photo-Responsive Molecules, Korea University
1-Anamdong, Seoul, 136-701 (Korea)
Fax: (+82) 2-3290-3544
E-mail: chobr@korea.ac.kr

[b] *H.-J. Choo, Prof. Dr. Y.-G. Ko*
Graduate School of Life Sciences and Biotechnology
Korea University (Korea)

[c] *C. H. Kim, T. Joo*
Department of Chemistry, Pohang University of Science and Technology
Pohang (Korea)
E-mail: thjoo@postech.ac.kr

[d] *Dr. H. M. Kim*
Present address: Department of Chemistry, Ajou University
Suwon, 443-749 (Korea)

Supporting information for this article is available on the WWW under http://www.chembiochem.org or from the author.

Results and Discussion

Synthesis

CH and CS were prepared in 30–40% overall yields from **1** and **3** by the same procedure as reported for CL (Scheme 1).[16] Reactions of **4** and **6** with methyl bromoacetate followed by hydrolysis afforded CH and CS.

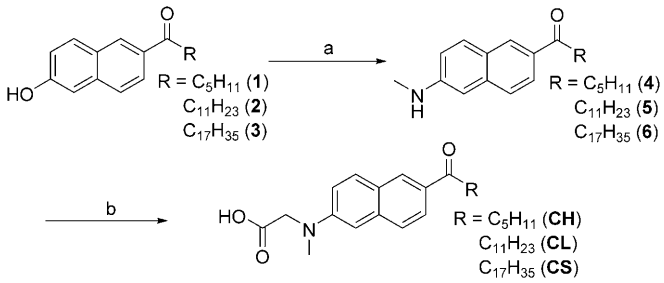

Scheme 1. a) $Na_2S_2O_5$/$MeNH_2HCl$/NaOH/H_2O; b) i: $BrCH_2CO_2CH_3$/proton-sponge/MeCN, ii: KOH/EtOH.

Spectroscopic properties in solution and model membranes

To assess the feasibility of using these compounds as TP probes for membrane lateral heterogeneity, we investigated following requirements: 1) sufficient water solubility for staining without the formation of aggregates within the cell, 2) environment-sensitive fluorescence, 3) capability to distinguish the liquid ordered (l_o) and liquid disordered (l_d) domains in the membrane, and 4) a significant two-photon cross-section in the 700–1000 nm range, which is necessary to obtain a clear TPM image at low dye concentration.

The water solubilities of CH and CS were determined by measuring their fluorescence intensities as a function of concentration.[16] The solubility decreases as the alkyl group chain length increases (CH(20 μM) > CL(3.0 μM) > CS(~0 μM), see Figure S1 in the Supporting Information. This indicates that introducing carboxylic acid moiety provides water solubility if the alkyl group chain length is not too long.

The sensitivity of the probes to the polarity of the environment has been assessed by comparing the emission spectra in different solvents and model membranes. The fluorescence spectra of CH and CL show gradual bathochromic shifts with increasing solvent polarity (cyclohexane < DMF < EtOH < H_2O, see Figure 1 A and B). The λ^{fl}_{max} increases by more than 100 nm as the solvent is changed from cyclohexane to water; this indicates a high sensitivity to solvent polarity. A similar result is observed for CS, although the emission is too weak to measure the λ^{fl}_{max} in H_2O due to its poor solubility (Figure 1 C and Table 1).

The emission spectra of the probes in the model membranes were significantly influenced by the alkyl group chain length. The spectra of CH in 1,2-dipalmitoyl-*sn*-glycero-3-phosphocholine (DPPC, gel phase, L_β),[18,19] DPPC/40 mol% CHL (l_o)[18,19] and 1,2-dioleoyl-*sn*-glycero-3-phosphocholine (DOPC)/sphingomyelin (SM)/CHL (1:1:1, raft mixture, $l_o + l_d$)[20–22] show a main band at 510–514 nm and a shoulder at 438 nm. The former can be attributed to the probes in water, as it shows the same λ^{fl}_{max} as those in water, whereas the latter is most

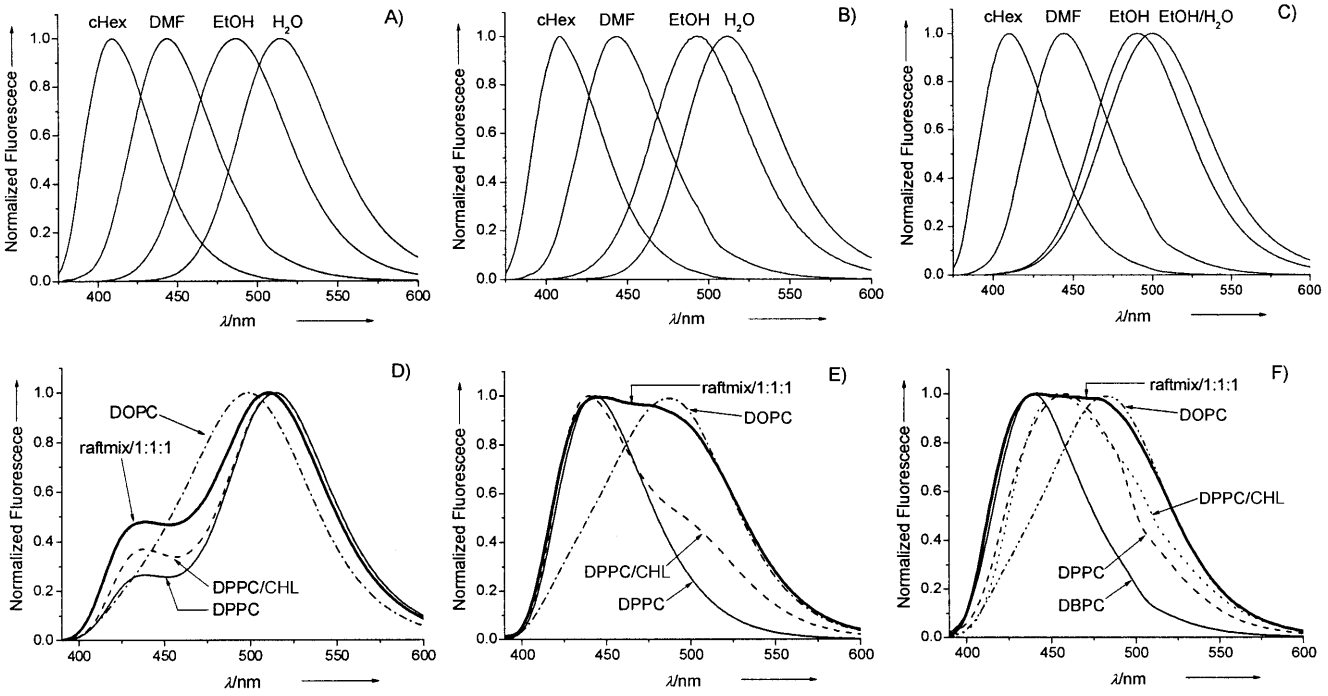

Figure 1. Normalized emission spectra of (A) CH, (B) CL and (C) CS in cyclohexane, DMF, EtOH, and H_2O. Normalized emission spectra of (D) CH and (E) CL in the phospholipid vesicles composed of DPPC, DPPC/40 mol% cholesterol, DOPC/sphingomyelin/cholesterol (1:1:1), and DOPC at 25 ± 0.5 °C. F) Normalized emission spectra of CS in the same vesicles and DBPC.

Table 1. Spectral data of CH, CL and CS.

Solvent	$\lambda_{max}^{(I)[a]}$			$\lambda_{max}^{fl\ [b]}$			$\Phi^{[c]}$			$\lambda_{max}^{(2)[d]}$			$\delta_{max}^{[e]}$			$\Phi\delta_{max}^{[f]}$		
	CH	CL	CS	CH	CL	CS	CH	CL	CS	CH	CL	CS	CH	CL	CS	CH	CL	CS
c-Hex	349	348	347	409	409	410	0.08	0.10	0.07									
DMF	370	369	372	444	444	444	0.18	0.36	1.00	780	780	780	190	170	90	35	60	90
EtOH	383	385	383	493	493	492	0.33	0.43	0.96	780	780	780	150	150	85	50	65	80
H_2O	382	381	344	515	512	nd	0.41	0.11	nd									

[a,b] λ_{max} of the one-photon absorption and emission spectra in nm. [c] Fluorescence quantum yield. [d] λ_{max} of the two-photon excitation spectra in nm. [e] The peak two-photon absorptivity in 10^{-50} cm^4 s/photon (GM). The experimental uncertainty is of the order of 10-15%. [f] Two-photon action cross-section. The values for CL are taken from ref. 16.

likely due to the probes in the rigid domain (Figure 1D). In vesicles composed of DOPC (l_d),[22] CH shows a λ_{max}^{fl} at 499 nm, similar to those of CL and CS in DOPC (Figure 1E and F). This limits the utility of CH as a membrane probe because it neither exclusively resides in the membrane nor equally represents the l_o and l_d domains. This is presumably due to its shorter alkyl group chain length, which increases water solubility and decreases hydrophobic interactions.

On the other hand, the emission spectra of CL show discrete λ_{max}^{fl} at 443 and 486 nm in DPPC/CHL and DOPC, respectively (Figure 1e). Moreover, the emission spectrum of the CL in the raft mixture is broad and almost the same as the sum of the spectra in DPPC/CHL and DOPC; this indicates that CL equally reflects the l_o and l_d domains in the vesicles.

The emission spectrum of CS in DOPC is nearly identical to that of CL despite the longer chain length of CS. In DPPC/CHL, however, CS shows appreciable bathochromic shift compared with CL. This indicates that the fluorophore of CS might be located closer to the hydrophilic lipid head groups probably because it is positioned away from the hydrocarbon layer of DPPC/CHL due to the longer alkyl groups. This interpretation is supported by the nearly identical λ_{max}^{fl} of CS in 1,2-dibehenoyl-*sn*-glycero-3-phosphocholine (DBPC) and CL in DPPC/CHL (Figure 1E and F). It is to be noted that the probes experience a similar environment when embedded in lipids with similar hydrocarbon lengths. Moreover, the emission spectrum of CS in the raft mixture is broad and almost the same as the sum of the spectra in DBPC and DOPC, that is, CS accurately reflects the rigid and fluid domains in the vesicles. This can be attributed to the favorable interactions between the carboxylate moiety of CS and water molecules near the lipid head group,[16] which may lead to the homogeneous distribution of CS in the model membrane and thus avoid aggregation. The observation of the photoselection effect in all of the GUVs labeled with CS is consistent with this interpretation (vide infra). For direct information about the probe location, quenching experiments might be needed.[23]

A similar temperature-dependent result was observed in the raft mixture. As the vesicles were gradually heated from 15 to 25 to 45 °C, the λ_{max}^{fl} of CH remained the same at 510 nm, whereas the shoulder at 438 nm decreased. This is expected, as the vesicles should become more fluid at a higher temperatures. Moreover, the spectra of CL and CS at 25 °C are broad and almost the same as the sum of the spectra at 15 and 45 °C (Figure S2); this provides additional evidence for the usefulness of these probes.

The emission spectrum of CS in 293T cells is similar to that of CS in DPPC/CHL, except that it is broader (Figure S3). This indicates that the polarity of the cell is similar to the polarity of DPPC/CHL, although the cell interior is more heterogeneous.[24] Upon treatment with MβCD, the spectrum red-shifts. The value of λ_{max}^{fl} was found to be between the values observed for DPPC/CHL and DOPC (Figure S3).

Time-resolved fluorescence (TRF) allows the study of the interactions that take place between the fluorophore excited state and its environment as well as their dynamics.[16,25] We have measured TRF to account for the spectral differences of laurdan and related compounds in different vesicles. It is well established that the sensitivity of the probe molecules to the dipolar nature of the environment originates from the intramolecular charge transfer (ICT) and the solvation of the ICT state.[16,26,27] In this case, the emission may originate from the locally excited (LE) state, the ICT state before solvation (ICT*), and the ICT state after the solvation (dielectric relaxation). For laurdan in vesicles, however, Parasassi et al.[28] argued against the LE/ICT model, and suggested that the LE state does not contribute to the emission spectrum; this implies that the initially excited state is the charge transfer state. Here, we adopt the LE/ICT model, as it satisfactorily accounts for all the stationary and time-resolved fluorescence data presented here and in our previous work.[16] In addition, an ICT process was also observed for laurdan in vesicles in a TRF study.[27] Nevertheless, the blue emission may still originate from both LE and ICT*, although the red emission must be due to the ICT/solvation process.

The ICT/solvation process can be best demonstrated by an increase in the TRF signal detected at the long wavelengths of the emission spectrum. The TRFs of CS (Figure S4 and Table S1) in DPPC/CHL are qualitatively different from those in other vesicles; this indicates that the environment surrounding the chromophore in DPPC/CHL is very different from the environment surrounding it in other vesicles. For other vesicles, however, the TRFs of CL and CS display similar results, as expected from the stationary spectra. The TRF of CS in DBPC shows that it does not undergo ICT/solvation or emit from the LE/ICT* state, whereas CS in DOPC and raft mixture undergoes ICT/solvation to give the red shifted emission spectra. In DOPC, the ICT/solvation process and the population decay of the LE state

are faster than those in the the raft mixture to give rise to a red emission band almost exclusively. In the raft mixture, however, the emission occurs from both the LE/ICT* and ICT states, which results in a broad spectrum. Similar results were reported for CL in vesicles.[16] Thorough inspection, however, reveals some differences. In DOPC, the ICT/solvation of CS is faster (90 ps) than that of CL (330 ps) and has a slightly weaker intensity at 430 nm, which is the wavelength at which the LE/ICT* emits (Figure 1 E and F). Also, ICT/solvation does not occur for CS in DBPC, whereas a small portion of CL in DPPC undergoes ICT/solvation. These results indicate that the environment around CS in DBPC is more homogeneous than that of CL in DPPC.

Although the emission spectra of CL and CS in DPPC and DPPC/CHL are similar, the addition of CHL makes the GUVs more fluidic, which results in an increase of the emission around 510 nm due to the ICT/solvation processes. The influence of CHL on the emission spectra, however, is smaller for CS than it is for CL as shown in Figure 1. The TRF data are also consistent with the stationary emission spectra. The TRF of CL in DPPC/CHL shows a rise when detected at 490 nm, whereas no rise component was observed for CL in DPPC. In addition, the TRF at 490 nm for CS in DPPC/CHL (Figure S4) does not show a noticeable rise component.

The TRFs of CS embedded in cells (Figure S5 and Table S1) do not show a rise component at 490 nm indicating that the ICT/solvation does not occur for CS. This is in sharp contrast to CL embedded in cells, in which a solid ICT/solvation was observed. Also, CS embedded in cells shows rather weak wavelength dependence. Thus, we expect that the GP distribution curves for CS will be narrower than those for CL. Treatment with MβCD, which destroys lipid rafts, removes the fast (100 ps) decay component, and the wavelength dependence becomes similar to that in DOPC. Interestingly, TRFs of CS embedded in cells are quite similar to TRF in DPPC/CHL and suggest that the environments for the chromophore in both samples are similar. (Most of the CS is located in l_o-like domains of cells, where the environment for CS is close to that for CS in DPPC/CHL). This in turn suggests that l_o-like domains in the cells are very similar to vesicles composed of DPPC/CHL. The close resemblance of the fluorescence spectra of CS in DPPC/CHL and cells corroborates this conclusion (Figure S3).

The two-photon cross-sections (δ_{TPA}) of CH, CL, and CS in ethanol are in the range of 85–150 GM (1 GM = 10^{-50} cm^4 s/photon) at 780 nm. Similar values were obtained in DMF (Table 1, Figure S7). In H_2O, the δ_{max} value of CL is 320 GM at 820 nm, whereas that of CS could not be measured due to its insolubility. Moreover, the two-photon action cross-sections of these probes are in the range of 35–90 GM in DMF and ethanol, which are sufficient to obtain bright images by TPM (Table 1).

Two-photon excitation with polarized light provides detailed information about the location of the probes in the bilayer.[16,29] Giant unilamellar vesicles (GUVs) composed of DPPC, DPPC/CHL, DOPC/SM/CHL (1:1:1 or 2:2:1)[30,31] or DOPC revealed a weak fluorescent area perpendicular to the excitation polarization (Figure S8). This shows that the probes are located parallel to the lipid molecules (the photoselection effect). This outcome can be attributed to the favorable hydrophilic interactions between the carboxylates and the water molecules near the lipid head groups in addition to the hydrophobic interactions between the probes and lipid molecules. This result underlines the importance of the carboxylic acid moiety oriented as parallel alignment in both fluid and rigid domains in the membrane (vide supra).

GP images of model membranes

The sensitivity of the probes to the membrane polarity was assessed by using generalized polarization (GP) images.[16,32–38] The GP values have been calculated by using Equation (1), where $I_{(400–460)}$ and $I_{(470–530)}$ are the fluorescence intensities at 400–460 nm and 470–530 nm, respectively, and G is the sensitivity correction factor of the two different wavelength ranges (see the Experimental Section).[16,37,38]

The GP images of the equatorial sections of GUVs labeled with CH, CL, and CS reveal GP values ranging from −0.45 to 0.42 (Figure 2 and Table 2). In DPPC, the GP distribution curves are narrow and the center GP values are 0.20, 0.41, and 0.37 for CH, CL, and CS, respectively (Figure 2 and Table 2). The much smaller GP value for CH indicates that it over-represents the l_d domain because of the shorter alkyl group chain length (vide supra). On the other hand, the center GP value of CS in DBPC GUVs is 0.42, which is nearly identical to that of CL in DPPC. In other words, the probes experience similar environment when embedded in lipids with similar hydrocarbon lengths (vide supra). In DPPC/CHL, the GP distribution curves are similar to those obtained in DPPC. The center GP values in DPPC/CHL are slightly smaller than those in DPPC (0.12, 0.32, 0.27 for CH, CL, and CS, respectively), due to the slight increase in fluidity (Figure 2 and Table 2). Moreover, the GP distribution curves are broader in DOPC than in DPPC/CHL, with center GP values of −0.45, −0.35, and −0.34 for CH, CL, and CS, respectively (Figure 2 and Table 2). Also, the GP value of CH is smaller than others; it over-represents the l_d domain (vide supra). In contrast, the center $|GP|$ values of CL and CS in DOPC are similar to those in DPPC/CHL; this indicates that CL and CS can equally represent the l_d and l_o domains.

Similar results were observed in the raft mixture. The GP distribution curve of CH-labeled GUVs is skewed toward the low GP region (Figure 2), whereas it is more symmetrical when stained with CL and CS (Figure 2). When the GP curves for CH-, CL-, and CS-labeled GUVs are fitted to a bimodal distribution, the center GP values are −0.17/0.08, −0.14/0.18, and −0.13/0.17, respectively (Table 2). The center GP values of CH are smaller than others, and the low GP distribution curve of CH is much broader than the high one (Figure 2), which limits its utility as the membrane probe. In contrast, the $|GP|$ values and the widths of the low and high GP curves for the CL- and CS-labeled GUVs are alike, indicating that they can reflect the two domains more accurately (Figure 2 and Table 2).

In DOPC/SM/CHL (2:2:1),[30,31] the emission spectra of all compounds are nearly the same as those measured in the raft mixture, except that there is an appreciable decrease in the

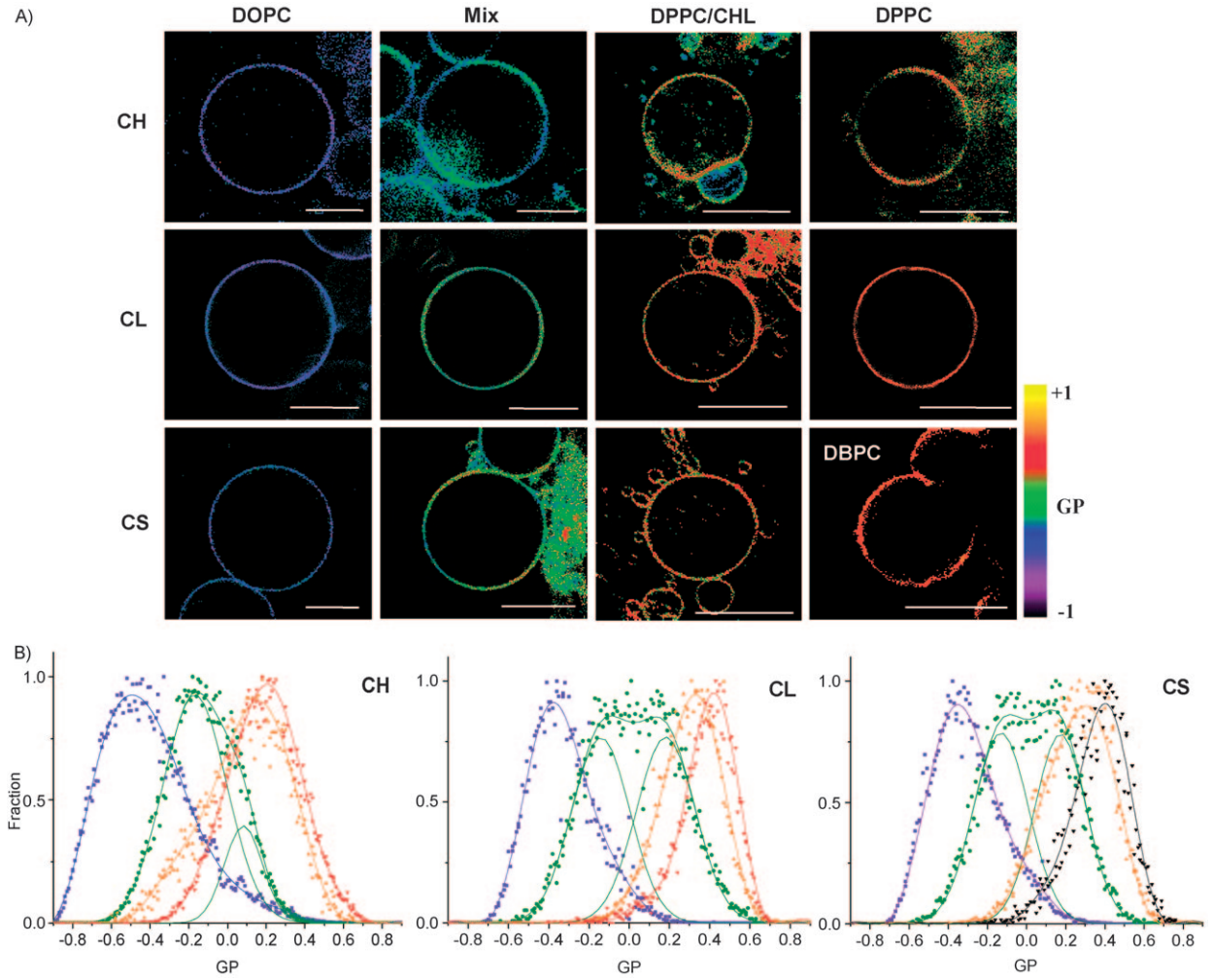

Figure 2. A) GP images of the equatorial section of single GUVs composed of DOPC, DOPC/sphingomyelin/cholesterol (1:1:1), DPPC/40 mol% cholesterol, DPPC, and DBPC labeled with CH, CL and CS at 25±0.5 °C. Scale bars, 30 μm. The images for CL are taken from Ref. [15] except for DPPC/cholesterol. B) GP distribution curves of DOPC (purple), DPPC/cholesterol (orange), DPPC (red) and DBPC (black) fitted to single component and of DOPC/sphingomyelin/cholesterol (1:1:1) fitted to bimodal distribution (green). The curves for CL are taken from ref. 16 except for DPPC/cholesterol.

Table 2. Two Gaussian distributions of deconvoluted stacks of GP images.

Sample	Probe	Center 1[a]	Width 1[b]	Center 2[c]	Width 2[d]	Coverage 2, %
DOPC	CH	−0.45 (0.003)[e]	0.44 (0.007)[e]			
	CL	−0.35 (0.003)[e]	0.32 (0.006)[e]			
	CS	−0.34 (0.002)[e]	0.36 (0.005)[e]			
raft mixture	CH	−0.17 (0.083)	0.33 (0.010)	0.08 (0.009)	0.20 (0.016)	26
	CL	−0.14 (0.012)	0.29 (0.014)	0.18 (0.012)	0.29 (0.014)	
	CS	−0.13 (0.019)	0.28 (0.018)	0.17 (0.017)	0.26 (0.015)	24
DPPC/40 mol% CHL	CH			0.12 (0.003)[e]	0.44 (0.006)[e]	
	CL			0.32 (0.002)[e]	0.30 (0.004)[e]	
	CS			0.27 (0.002)[e]	0.35 (0.004)[e]	
DPPC	CH			0.20 (0.002)[e]	0.39 (0.005)[e]	
	CL			0.41 (0.001)[e]	0.24 (0.003)[e]	
	CS			0.37 (0.002)[e]	0.36 (0.005)[e]	
DBPC	CS			0.42 (0.003)[e]	0.26 (0.006)[e]	
293T Cell	CL	−0.037 (0.015)	0.36 (0.016)	0.33 (0.014)	0.34 (0.014)	31
	CL-MβCD	−0.001 (0.042)	0.43 (0.040)	0.28 (0.044)	0.28 (0.080)	9
	CS	−0.070 (0.006)	0.25 (0.007)	0.22 (0.005)	0.27 (0.007)	35
	CS-MβCD	−0.055 (0.009)	0.31 (0.012)	0.17 (0.005)	0.18 (0.010)	14

[a–d] The center GP values of low- and high-GP regions and their width in the GP curves fitted to two Gaussian distributions except otherwise noted. The numbers in the parenthesis are the standard deviation. [e] The center GP values and their width in the GP curves fitted to single component. [f] DOPC/sphingomyelin/cholesterol (1:1:1) and the values for CL are taken from ref. [16], except for DPPC/cholesterol.

shorter wavelength bands due to the enhanced fluidity (Figure S9). Moreover, the GP images of the GUVs labeled with all compounds revealed the discrete domains of l_o and l_d phases with the center GP values of −0.34/0.11, −0.34/0.34, and −0.29/0.29, respectively (Figure S10). Here again, CH over-represents the l_d domain, while CL and CS equally reflect both domains.

The combined results reveal that CL and CS are useful two-photon probes for the lipid rafts as they can exclusively reside in the membrane, equally reflect the l_d and l_o domains in the model membrane, and exhibit significant two-photon action cross-sections.

GP images of cells

TPM images of the CL- and CS-labeled 293T cells reveal that CS is preferentially located in the plasma membrane (Figure 3c), whereas CL is distributed in both plasma membrane and cytosol (Figure 3a). The high and low GP curves of CL are symmetrical and well separated from the intersection at 0.15; this probe equally reflects l_d- and l_o-like domains in the cells. On the other hand, the high GP curve of CS is appreciably taller than the low one, indicating that it has a greater tendency to be located in the l_o-like domains of the cell as revealed by TRF experiment (vide supra). When the cells were treated with MβCD, a drug that destroys the lipid raft by removing CHL from the plasma membrane, the high GP curve, centered at GP = 0.22–0.33, decreased significantly while no alteration was observed in the low GP curve (Figure 3b,f and 3d,h, Table 2). Therefore, the high GP domain can readily be attributed to the l_o-like domains.

To unambiguously determine whether the high GP domains in the CL- and CS-labeled cells are indeed the l_o-like domains, the high GP images were co-localized with the fluorescence image of ganglioside G_{M1}, which is known to be highly enriched in the raft domains,[39] by co-staining the cells with CL (or CS) and BODIPY-G_{M1}. As shown in Figure S11c and S11f, the two images merged well, confirming that the high GP image reflects the l_o-like domains. Hence, the direct visualization of the membrane lateral heterogeneity is clearly shown with TPM by using CL and CS as the probes. Therefore, it can be concluded that CL and CS are useful two-photon probes that can represent the l_d and l_o domains in the cell membrane. Of these two, CS can better reflect the plasma membrane. These results underline the importance of alkyl group chain length and the head group carboxylic acid moiety for the design of efficient two-photon probes of membrane lateral heterogeneity.

To demonstrate the utility of these probes, TPM images were obtained of individual 293T cells labeled with 2 μM CL and CS. The GP distribution curves of each section of the cells reveal that the GP value increases gradually from bottom to the top of the cells (Figures S12 and S13). The total surface areas covered by high GP domains of CL- (GP > 0.33) and CS-labeled (GP > 0.28) cells are 31 and 35%, respectively. When the cells were treated with MβCD, the value decreased to 9 and 14%, respectively. These results indicate that the l_o-like domains cover 31–35% of the cell surface and are enriched on the top edge of the cell. A similar value was reported for CL-labeled A431 cells.[16]

Conclusions

A series of two-photon probes have been developed based on 6-acyl-2-aminonaphthalene as the fluorophore and hexanoyl, lauryl, stearyl groups as the receptor for the membrane and their photophysical properties as well as their utility as the

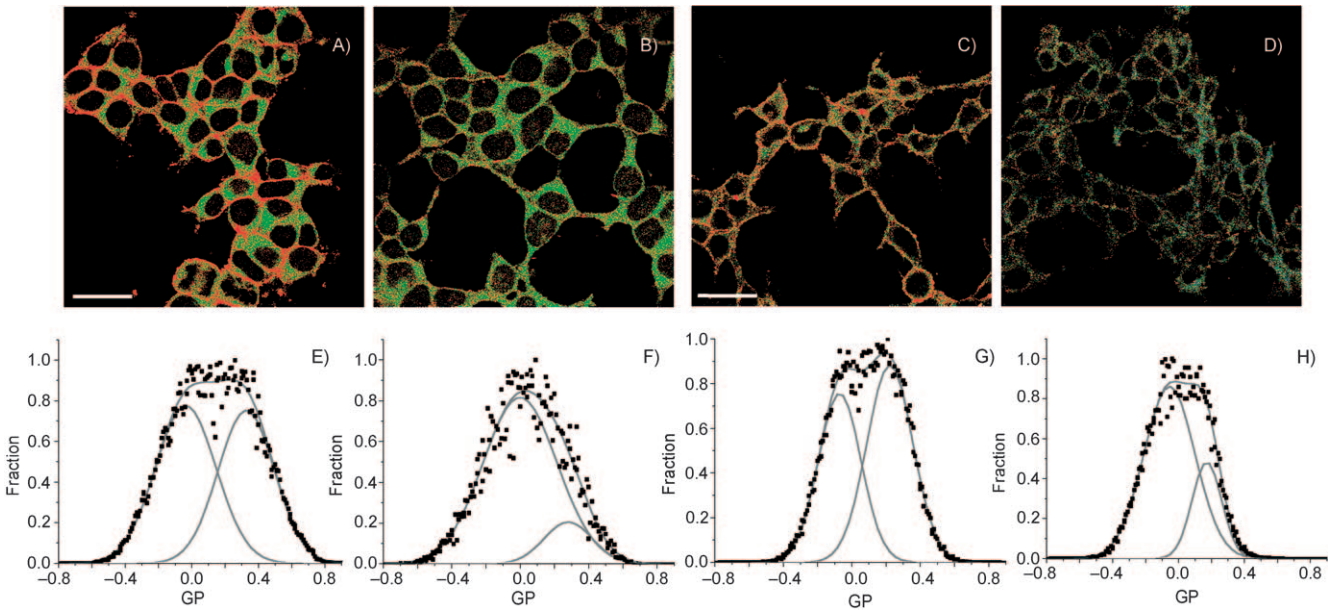

Figure 3. GP images of CL-labeled 293T cells A) before and B) after treatment with 10 mM MβCD for 30 min. GP images of the CS-labeled 293T cells C) before and D) after treatment with MβCD. Scale bar, 30 μm. GP distribution curves of CL-labeled 293T cells E) before and F) after treatment. GP distribution curves of CS-labeled 293T cells G) before and H) after treatment.

membrane probe were studied. The results show that CH cannot be used as the membrane probe because it neither exclusively resides in the membrane nor equally represent the l_d and l_o domains. On the other hand, CL and CS are excellent two-photon probes for the membrane because they can equally reflect the two domains and are capable of imaging the membrane lateral heterogeneity in live cells. Moreover, CS has a greater tendency to be located in the plasma membrane due to the poor water solubility, whereas CL partitions into both plasma membrane and cytosol. Finally, our results show that the l_o-like domains cover 31–35% of the cell surface.

Experimental Section

Synthetic reagents were purchased from Sigma–Aldrich and used without further purification. All solvents were from Riedel–de Haën (Seelze, Germany) and Sigma–Aldrich and were distilled prior to use. DPPC, DOPC, and SM were from Avanti Polar Lipids (Alabaster, AL, USA). CHL was from Sigma–Aldrich. Synthesis of C-laurdan was reported previously.[16] Synthesis of other compounds is described below.

6-Hexanoyl-2-methoxynaphthalene was synthesized using a previously published method.[40] 2-Methoxynaphthalene (10.0 g, 63.2 mol) was added to a solution containing $AlCl_3$ (10.1 g, 75.9 mmol) in nitrobenzene (150 mL). Distilled hexanoyl chloride (10.4 mL, 75.9 mmol) was slowly added to this solution with stirring at 10–13 °C. After addition of the hexanoyl chloride was completed, the mixture was stirred at 5 °C for 2 h and then room temperature for 12 h. The reaction mixture was cooled in an ice bath, poured into ice water (300 mL), and treated with HCl (50 mL of 35%, aq). The product was extracted with chloroform, excess nitrobenzene was removed in vacuo, and the product was purified by crystallization from MeOH. Yield 10.7 g (66%); m.p. 67 °C; IR (KBr): 1664 cm^{-1}; ^1H NMR (300 MHz, $CDCl_3$): $\delta = 8.40$ (d, $J = 2$ Hz, 1H), 8.02 (dd, $J = 9$, $J = 2$ Hz, 1H), 7.85 (d, $J = 9$ Hz, 1H), 7.76 (d, $J = 9$ Hz, 1H), 7.20 (dd, $J = 9$, $J = 2$ Hz, 1H), 7.15 (d, $J = 2$ Hz, 1H), 3.95 (s, 3H), 3.07 (t, $J = 7.5$ Hz, 2H), 1.79 (quint, $J = 7.5$ Hz, 2H), 1.40 (m, 4H), 0.93 (t, $J = 7.5$ Hz, 3H); elemental analysis calcd (%) for $C_{17}H_{20}O_2$: C 79.65, H 7.86; found: C 79.42, H 7.56.

6-Octadecanoyl-2-methoxynaphthalene was obtained in 53% overall yield from 2-methoxynaphthalene and octadecanoyl chloride according to above procedure for 6-hexanoyl-2-methoxynaphthalene. m.p. 88 °C; IR (KBr): 1663 cm^{-1}; ^1H NMR (300 MHz, $CDCl_3$): $\delta = 8.40$ (d, $J = 2$ Hz, 1H), 8.01 (dd, $J = 9$, $J = 2$ Hz, 1H), 7.85 (d, $J = 9$ Hz, 1H), 7.76 (d, $J = 9$ Hz, 1H), 7.20 (dd, $J = 9$, $J = 2$ Hz, 1H), 7.16 (d, $J = 2$ Hz, 1H), 3.95 (s, 3H), 3.06 (t, $J = 7.5$ Hz, 2H), 1.78 (quint, $J = 7.5$ Hz, 2H), 1.34 (m, 28H), 0.88 (t, $J = 7.5$ Hz, 3H); elemental analysis calcd (%) for $C_{29}H_{44}O_2$: C 82.02, H 10.44; found: C 82.52, H 10.26.

6-Hexanoyl-2-hydroxynaphthalene (**1**). HBr (48%, 58.4 g, 0.72 mol) was added to a solution containing 6-hexanoyl-2-methoxynaphthalene (8.4 g, 32.8 mmol) in glacial acetic acid (300 mL). The mixture was stirred at 100 °C for 12 h. Excess acetic acid was removed in vacuo, and the residue was taken up in ethyl acetate and washed with dilute $NaHCO_3$ and brine. The organic layer was dried with $MgSO_4$ and the solvent was removed in vacuo. The product was purified by column chromatography using ethyl acetate/hexane (1:3). Yield 5.7 g (72%); m.p. 148 °C; IR (KBr): 3360, 1664 cm^{-1}; ^1H NMR (300 MHz, $CDCl_3$): $\delta = 8.41$ (d, $J = 2$ Hz, 1H), 7.99 (dd, $J = 9$, $J = 2$ Hz, 1H), 7.87 (d, $J = 9$ Hz, 1H), 7.70 (d, $J = 9$ Hz, 1H), 7.19 (d, $J = 2$ H, 1Hz), 7.18 (dd, $J = 9$, $J = 2$ Hz, 1H), 5.44 (br s, 1H), 3.07 (t, $J = 7.5$ Hz, 2H), 1.79 (quint, $J = 7.5$ Hz, 2H), 1.40 (m, 4H), 0.92 (t, $J = 7.5$ Hz, 3H); elemental analysis calcd (%) for $C_{16}H_{18}O_2$: C 79.31, H 7.49; found: C 79.72, H 7.16.

6-Octadecanoyl-2-hydroxynaphthalene (**3**) was obtained in 58% overall yield from 6-octadecanoyl-2-methoxynaphthalene according to above procedure of **1**. m.p. 100 °C; IR (KBr): 3362, 1662 cm^{-1}; ^1H NMR (300 MHz, $CDCl_3$): $\delta = 8.41$ (d, $J = 2$ Hz, 1H), 7.99 (dd, $J = 9$, $J = 2$ Hz, 1H), 7.87 (d, $J = 9$ Hz, 1H), 7.71 (d, $J = 9$ Hz, 1H), 7.18 (d, $J = 2$ Hz, 1H), 7.17 (dd, $J = 9$, $J = 2$ Hz, 1H), 5.43 (br s, 1H), 3.06 (t, $J = 7.5$ Hz, 2H), 1.78 (quint, $J = 7.5$ Hz, 2H), 1.29 (m, 28H), 0.89 (t, $J = 7.5$ Hz, 3H); elemental analysis calcd (%) for $C_{28}H_{42}O_2$: C 81.90, H 10.31; found: C 81.22, H 10.86.

6-Hexanoyl-*N*-methyl-2-naphthylamine (**4**). $MeNH_2$·HCl (7.6 g, 93.0 mol) was added to a mixture of **1** (4.5 g, 18.6 mmol), $Na_2S_2O_5$ (7.1 g, 37.2 mmol), NaOH (3.7 g, 93.0 mmol), and H_2O (100 mL) in a pressure tube and the mixture was stirred at 140 °C for 72 h. The product was collected by filtration, washed with water, and purified by column chromatography using ethyl acetate/toluene (1:50) as the eluent. Yield 2.9 g (61%); m.p. 121 °C; IR (KBr): 3360, 1663 cm^{-1}; ^1H NMR (300 MHz, $CDCl_3$): $\delta = 8.31$ (d, $J = 2$ Hz, 1H), 7.93 (dd, $J = 9$, $J = 2$ Hz, 1H), 7.71 (d, $J = 9$ Hz, 1H), 7.63 (d, $J = 9$ Hz, 1H), 6.91 (dd, $J = 9$, $J = 2$ Hz, 1H), 6.77 (d, $J = 2$ Hz, 1H), 4.14 (br s, 1H), 3.03 (t, 2H, $J = 7.5$ Hz), 2.97 (s, 3H), 1.79 (quint, 2H, $J = 7.5$ Hz), 1.39 (m, 4H), 0.92 (t, $J = 7.5$ Hz, 3H); elemental analysis calcd (%) for $C_{17}H_{21}NO$: C 79.96, H 8.29, N 5.49; found: C 79.26, H 8.55, N 5.70.

6-Octadecanoyl-*N*-methyl-2-naphthylamine (**6**) was obtained in 48% overall yield from **2** according to above procedure of **3**. m.p. 96 °C; IR (KBr): 3376, 1663 cm^{-1}; ^1H NMR (300 MHz, $CDCl_3$): $\delta = 8.31$ (d, $J = 2$ Hz, 1H), 7.94 (dd, $J = 9$, $J = 2$ Hz, 1H), 7.73 (d, $J = 9$ Hz, 1H), 7.64 (d, $J = 9$ Hz, 1H), 6.96 (dd, $J = 9$, $J = 2$ Hz, 1H), 6.86 (d, $J = 2$ Hz, 1H), 4.10 (br s, 1H), 3.03 (t, $J = 7.5$ Hz, 2H), 2.98 (s, 3H), 1.77 (quint, $J = 7.5$ Hz, 2H), 1.28 (m, 28H), 0.88 (t, $J = 7.5$ Hz, 3H); elemental analysis calcd (%) for $C_{29}H_{45}NO$: C 82.21, H 10.71, N 3.31; found: C 82.08, H 10.77, N 3.71.

CH. Methyl bromoacetate (1.4 g, 8.8 mmol), **4** (1.5 g, 5.9 mmol), and proton sponge (1.9 g, 8.8 mmol) in MeCN (50 mL) were refluxed under N_2 for 18 h. The product was extracted with ethyl acetate, washed with brine, and purified by crystallization from EtOH to obtain light yellow powder. Yield 1.4 g (72%); m.p. 76 °C; ^1H NMR (300 MHz, $CDCl_3$): $\delta = 8.33$ (d, $J = 2$ Hz, 1H), 7.94 (dd, $J = 9$, $J = 2$ Hz, 1H), 7.81 (d, $J = 9$ Hz, 1H), 7.65 (d, $J = 9$ Hz, 1H), 7.09 (dd, $J = 9$, $J = 2$ Hz, 1H), 6.88 (d, $J = 2$ Hz, 1H), 4.22 (s, 2H), 3.74 (s, 3H), 3.20 (s, 3H), 3.03 (t, $J = 7.5$ Hz, 2H), 1.78 (quint, $J = 7.5$ Hz, 2H), 1.39 (m, 4H), 0.92 (t, $J = 7.5$ Hz, 3H). A mixture of this intermediate (0.8 g, 2.4 mmol) and KOH (1.0 g, 25 mmol) in EtOH (50 mL) was stirred for 5 h. The resultant solution was concentrated and diluted with ice-water (100 mL) and concentrated HCl (aq) was added slowly at < 5 °C until pH 3. The resulting precipitate was collected, washed with distilled water, and purified by crystallization from chloroform-petroleum ether. Yield 0.5 g (66%); m.p. 148 °C; ^1H NMR (300 MHz, $CDCl_3$): $\delta = 8.33$ (d, $J = 2$ Hz, 1H), 7.94 (dd, $J = 9$, $J = 2$ Hz, 1H), 7.81 (d, $J = 9$ Hz, 1H), 7.65 (d, $J = 9$ Hz, 1H), 7.10 (dd, $J = 9$, $J = 2$ Hz, 1H), 6.90 (d, $J = 2$ Hz, 1H), 4.25 (s, 2H), 3.20 (s, 3H), 3.04 (t, $J = 7.5$ Hz, 2H), 1.78 (quint, $J = 7.5$ Hz, 2H), 1.39 (m, 4H), 0.92 (t, $J = 7.5$ Hz, 3H); ^{13}C NMR (100 MHz, [D_6]DMSO): $\delta = 199.9$, 172.4, 149.8, 137.8, 131.5, 130.7, 130.6, 130.3, 125.5, 116.8, 116.6, 105.7, 105.4, 53.8, 38.1, 31.7, 24.6, 22.8, 14.6; IR (KBr): 3275–2420, 1710, 1663 cm^{-1}; elemental analysis calcd (%) for $C_{19}H_{23}NO_3$: C 72.82, H 7.40, N 4.47; found: C 72.60, H 7.76, N 4.54.

CS was obtained in 60% overall yield from **6** according to above procedure of C-hexadan. m.p. 69 °C; IR (KBr): 3285–2425, 1710, 1663 cm^{-1}; ^1H NMR (300 MHz, $CDCl_3$): $\delta = 8.32$ (d, $J = 2$ Hz, 1H), 7.93 (dd, $J = 9$, $J = 2$ Hz, 1H), 7.81 (d, $J = 9$ Hz, 1H), 7.65 (d, $J = 9$ Hz, 1H), 7.10 (dd, $J = 9$, $J = 2$ Hz, 1H), 6.91 (d, $J = 2$ Hz, 1H), 4.24 (s, 2H), 3.20 (s, 3H), 3.04 (t, $J = 7.5$ Hz, 2H), 1.76 (quint, $J = 7.5$ Hz, 2H), 1.29 (m, 28H), 0.87 (t, $J = 7.5$ Hz, 3H); ^{13}C NMR (100 MHz, $[D_6]$DMSO): $\delta =$ 200.6, 175.3, 151.5, 137.5, 131.2, 131.1, 129.7, 126.8, 125.3, 124.8, 115.8, 106.3, 100.2, 54.3, 40.1, 38.7, 30.2, 30.1, 30.0, 29.9, 29.8, 29.7, 29.6, 29.5, 29.4, 29.3, 29.2, 29.1, 25.2, 22.9, 14.6; elemental analysis calcd (%) for $C_{31}H_{47}NO_3$: C 77.29, H 9.83, N 2.91; found: C 77.81, H 9.98, N 2.54.

Spectroscopic measurements. Absorption spectra were recorded on a Hewlett–Packard 8453 diode array spectrophotometer, and the excitation and fluorescence spectra were obtained with Aminco Bowman series 2 luminescence spectrometer from Spectronics (USA) with excitation at 365 nm. A polarizer was placed in the emission path of the fluorometer to eliminate Wood's anomaly.[41] The fluorescence quantum yield was determined by using Coumarin 307 from (Exciton, Dayton, OH, USA) as a reference by the literature method.[42]

Time resolved fluorescence (TRF). Time correlated single photon counting (TCSPC) method was used to record picosecond TRF. Output of a home-built cavity-dumped Kerr lens mode-locked Ti: sapphire laser running at 760 nm was doubled to generate the excitation pulses at 380 nm. A 200 μm thick sample cuvette was installed on a home-made temperature-regulated cuvette holder. Fluorescence at the magic angle was detected by a thermoelectrically cooled microchannel plate photomultiplier tube (Hamamatsu, R3809U-51). Instrument response function has a width of 42 ps full width at half maximum to provide ~8 ps time resolution with deconvolution.

Water solubility. Water solubility was determined by adding small increments of the dye solution in DMSO to a cuvette containing H_2O (3.0 mL). In all cases, the DMSO content was maintained at 0.2%. The maximum concentration in the linear region in the plot of fluorescence intensity against the dye concentration was taken as the solubility (Figure S1).

Measurement of two-photon cross-sections. The two-photon cross-section (δ) was determined by using femtosecond fluorescence measurement technique as described by Lee.[43] Samples were dissolved in DMF (or EtOH) at concentrations of 5.0 μM and the two-photon induced fluorescence intensity was measured by using fluorescein (8.0×10^{-6} M, pH 11) as the reference, whose two-photon properties have been well characterized in the literature.[6]

Vesicle preparation. Vesicles for the measurements of one photon excitation and fluorescence spectra were prepared by the solvent evaporation method.[44] To grow GUVs, the electroformation method was employed.[16,45,46] An imaging chamber (designed for field stimulation, RC-21BRFS, Warner Instruments Co. (Hamden, CT, USA) modified for vesicle preparation (two parallel platinum electrodes separated between their surfaces 1 mm) was employed for this experiment. The temperature was measured inside the chamber at the platinum wires, using a digital thermometer with a precision of 0.1 °C. The probe in DMSO was added to the sample chamber after the vesicles were formed. The probe ratio in the vesicle was kept greater than 300:1.

Cells. 293T cells were cultured in Dulbecco's modified Eagle's medium supplemented with penicillin/streptomycin and fetal bovine serum (10%) in a CO_2 incubator at 37 °C. To test the co-localization of ganglioside G_{M1}, and high GP image of CS (or CL), 293T cells were treated with BODIPY-G_{M1} (150 nM, Molecular Probes) and CS or CL (2 μM) for 40 min at 4 °C, fixed with formaldehyde (3.7%), and observed in a spectral confocal multiphoton microscope.

One- and two-photon fluorescence microscopy. One- and two-photon fluorescence images were obtained with spectral confocal multiphoton microscopes (Leica TCS SP2) with a ×100 oil-immersion objective, numerical aperture (NA) = 1.30. For one-photon fluorescence microscopy, an Ar laser (488 nm excitation, 500–520 nm emission for BODIPY-G_{M1}) was used as the excitation source. Two-photon fluorescence microscopy images of the CL and CS-labeled GUVs and cells were obtained by exciting the probes with a mode-locked titanium-sapphire laser (780 nm, Coherent Chameleon, 90 MHz, 200 fs). To obtain images at various wavelengths, internal PMTs were used to collect the signals in an 8 bit unsigned 512×512 pixels at 400 Hz scan speed. The intensity images of CL and CS were recorded with the emission in the range of 400–460 nm and 470–530 nm with two channels of PMTs. The relative sensitivities of the two channels were determined for each experiment by using 0.5 μM CL and CS in DMSO, and the G-factor in Equation (1) was calculated. For GP function images, a quarter wave-plate was aligned and placed before the microscope to minimize the polarization effects of the excitation light.

GP image analysis. To quantify the emission spectral changes in the giant unilamellar vesicles (GUVs), the GP values in Equation 1 have been calculated for each pixel by measuring the fluorescence intensities at 400–460 nm and 470–530 nm.[16,37,38]

$$GP = \frac{I_{(400-460)} - G \times I_{(470-530)}}{I_{(400-460)} + G \times I_{(470-530)}} \quad (1)$$

Here, G is the sensitivity correction factor for the two different wavelength ranges. Background values, defined as less than 7% of the maximum intensity, were set to zero and colored black (float type). GP distributions were obtained from the histograms of GP values of the images and fitted to one or two Gaussian functions by the nonlinear fitting algorithm (Origin 7.0).

Acknowledgements

This work was supported by KOSEF 2008-01001 and R0A-2007-000-20027-0. TJ acknowledges the support by KOSEF R11-2007-012-01001-0.

Keywords: cells · c-steardan · fluorescent probes · membranes · two-photon microscopy

[1] M. D. Cahalan, I. Parker, S. H. Wei, M. J. Miller, *Nat. Rev. Immunol.* **2002**, *2*, 872–880.
[2] W. R. Zipfel, R. M. Williams, W. W. Webb, *Nat. Biotechnol.* **2003**, *21*, 1369–1377.
[3] F. Helmchen, W. Denk, *Nat. Methods* **2005**, *2*, 932–940.
[4] R. M. Williams, W. R. Zipfel, W. W. Webb, *Curr. Opin. Chem. Biol.* **2001**, *5*, 603–608.
[5] C. Xu, W. Zipfel, J. B. Shear, R. M. Williams, W. W. Webb, *Proc. Natl. Acad. Sci. USA* **1996**, *93*, 10763–10768.
[6] C. Xu, W. W. Webb, *J. Opt. Soc. Am. B* **1996**, *13*, 481–491.
[7] K. Simons, E. Ikonen, *Nature* **1997**, *387*, 569–572.
[8] K. Simons, D. Toomre, *Nat. Immunol. Nat. Rev. Mol. Cell. Biol.* **2000**, *1*, 31–39.
[9] S. Munro, *Cell* **2003**, *115*, 377–388.

[10] R. G. W. Anderson, *Annu. Rev. Biochem.* **1998**, *67*, 199–225.
[11] R. G. W. Anderson, K. Jacobson, *Science* **2002**, *296*, 1821–1825.
[12] M. Dykstra, A. Cherukuri, H. W. Sohn, S. J. Tzeng, S. K. Pierce, *Annu. Rev. Immunol.* **2003**, *21*, 457–481.
[13] F. Galbiati, B. Razani, M. P. Lisanti, *Cell* **2001**, *106*, 403–411.
[14] S. Mukherjee, F. R. Maxfield, *Annu. Rev. Cell Dev. Biol.* **2004**, *20*, 839–866.
[15] K. Jacobson, O. G. Mouritsen, R. G. W. Anderson, *Nat. Cell Biol.* **2007**, *9*, 7–14.
[16] H. M. Kim, H.-J. Choo, S.-Y. Jung, Y.-G. Ko, W.-H. Park, S.-J. Jeon, C. H. Kim, T. Joo, B. R. Cho, *ChemBioChem* **2007**, *8*, 553–559.
[17] D. A. Brown, E. London, *J. Biol. Chem.* **2000**, *275*, 17221–17224.
[18] M. B. Sankaram, T. E. Thompson, *Proc. Natl. Acad. Sci. USA* **1991**, *88*, 8686–8690.
[19] J. A. Clarke, A. J. Heron, J. M. Seddon, R. V. Law, *Biophys. J.* **2006**, *90*, 2383–2393.
[20] C. Dietrich, L. A. Bagatolli, Z. N. Volovyk, N. L. Thompson, M. Levi, K. Jacobson, E. Gratton, *Biophys. J.* **2001**, *80*, 1417–1428.
[21] M. Edidin, *Annu. Rev. Biophys. Biomol. Struct.* **2003**, *32*, 257–283.
[22] T. Baumgart, S. T. Hess, W. W. Webb, *Nature* **2003**, *425*, 821–824.
[23] M. B. Sankaram, T. E. Thompson, *Biochemistry* **1990**, *29*, 10670–10675.
[24] K.-B. Kim, J.-W. Lee, C. S. Lee, B.-W. Kim, H.-J. Choo, S.-Y. Jung, S.-G. Chi, Y.-S. Yoon, G. Yoon, Y.-G. Ko, *Proteomics* **2006**, *6*, 2444–2453.
[25] T. Parasassi, G. Ravagnan, R. M. Rusch, E. Gratton, *Photochem. Photobiol.* **1993**, *57*, 403–410.
[26] M. Viard, J. Gallay, M. Vincent, O. Meyer, B. Robert, M. Paternostre, *Biophys. J.* **1997**, *73*, 2221–2234.
[27] M. Viard, J. Gallay, M. Vincent, M. Paternostre, *Biophys. J.* **2001**, *80*, 347–359.
[28] T. Parasassi, E. K. Krasnowska, L. Bagatolli, E. Gratton, *J. Fluoresc.* **1998**, *8*, 365–373.
[29] L. A. Bagatolli, E. Gratton, *Biophys. J.* **2000**, *78*, 290–305.
[30] S. L. Veatch, S. L. Keller, *Biophys. J.* **2003**, *84*, 725–726.
[31] S. L. Veatch, S. L. Keller, *Biophys. J.* **2003**, *85*, 3074–3083.
[32] T. Parasassi, E. Gratton, W. M. Yu, P. Wilson, M. Levi, *Biophys. J.* **1997**, *72*, 2413–2429.
[33] L. A. Bagatolli, E. Gratton, *Biophys. J.* **1999**, *77*, 2090–2101.
[34] L. A. Bagatolli, E. Gratton, *Biophys. J.* **2000**, *79*, 434–447.
[35] L. A. Bagatolli, S. A. Sanchez, T. Hazlett, E. Gratton, *Methods Enzymol.* **2003**, *360*, 481–500.
[36] S. A. Sanchez, E. Gratton, *Acc. Chem. Res.* **2005**, *38*, 469–477.
[37] K. Gaus, E. Gratton, E. P. Kable, A. S. Jones, I. Gelissen, L. Kritharides, W. Jessup, *Proc. Natl. Acad. Sci. USA* **2003**, *100*, 15554–15559.
[38] K. Gaus, T. Zech, T. Harder, *Mol. Membr. Biol.* **2006**, *23*, 41–48.
[39] P. W. Janes, S. C. Ley, A. I. Magee, *J. Cell. Biol.* **1999**, *147*, 447–461.
[40] L. Arsenijevic, V. Arsenijevic, A. Horeau, J. Jacques, *Organic Syntheses*, Coll. Vol. 6, John Wiley and Sons, Inc., New York, N. Y., 1988, p. 34.
[41] D. Kessel, *Photochem. Photobiol.* **1991**, *54*, 481–483.
[42] J. N. Demas, G. A. Crosby, *J. Phys. Chem.* **1971**, *75*, 991–1024.
[43] S. K. Lee, W. J. Yang, J. J. Choi, C. H. Kim, S. J. Jeon, B. R. Cho, *Org. Lett.* **2005**, *7*, 323–326.
[44] A. Moscho, O. Orwar, D. T. Chiu, B. P. Modi, R. N. Zare, *Proc. Natl. Acad. Sci. USA* **1996**, *93*, 11443–11447.
[45] M. I. Angelova, D. S. Dimitrov, *Faraday Discuss. Chem. Soc.* **1986**, *81*, 303–311.
[46] F. M. Menger, M. I. Angelova, *Acc. Chem. Res.* **1998**, *31*, 789–797.

Received: May 26, 2008
Published online on October 30, 2008

